Electronic scattering in doped finite superlattices

A. B. Henriques
Instituto de Física, Universidade de São Paulo, Caixa Postal 66318, 05315-970 São Paulo, Brazil

P. L. Souza and B. Yavich
Centro de Estudos em Telecomunicações, Pontifícia Universidade Católica, Rua Marques de São Vicente, 225, 22453-900 Rio de Janeiro, Brazil

(Received 16 February 2001; published 2 July 2001)

The electronic scattering and momentum relaxation times for the individual levels in finite short-period modulation-doped superlattices were calculated, using the random phase approximation (RPA) to describe the screened electron-defect interactions. To obtain the highest possible electronic mobility, the donor impurities were placed in the middle of the barriers separating the wells. If the impurities are displaced from their ideal positions, the electronic mobility decreases. To evaluate the theory, measurements of the scattering and momentum relaxation times were done on InP/$In_{0.53}Ga_{0.47}As$ superlattices. Whereas theory and experiment agree fairly well on the values of the scattering times, the agreement on the momentum relaxation times is only in order of magnitude. This is attributed to the inexactness of the screened potential in the RPA at short distances from the scattering centers.

DOI: 10.1103/PhysRevB.64.045319 PACS number(s): 73.21.Cd, 73.20.−r

I. INTRODUCTION

Since the pioneering work by Esaki and Tsu,[1] semiconductor superlattices have attracted much interest due to the variety of interesting physical phenomena that can be observed in these systems—Bloch oscillations,[2] negative differential resistance,[3] and ballistic[4] and chaotic transport.[5] Superlattices are ideal systems for the investigation of quantum Hall phases in three dimensional conductors,[6] and they can be used for interesting device applications.[7] A key parameter in superlattices is the scattering time of the single particle states. The magnitude of the scattering time establishes the range of physical phenomena that can be observed, and it is determined by the efficiency of the scattering mechanisms in operation. For undoped superlattices, scattering is dominated by interface roughness, and the scattering time is 1 ps in $GaAs/Al_xGa_{1-x}As$ structures.[4] The purpose of this work is to investigate the scattering time of the single particle states in heavily doped superlattices, when electron–ionized-impurity interaction is the dominant scattering mechanism. The screening of the scattering potential is treated in the random phase approximation (RPA), which has been previously applied to multisubband systems with success.[8,9] The electronic scattering and momentum relaxation times are studied as a function of the number of layers in the superlattice, the thickness of the layers, the density of dopants, and the spatial distribution of the doping atoms. To maximize the electronic mobility, the doping atoms are placed in the middle of the potential barriers separating the wells. At sufficiently high densities Tamm states are formed, due to the finite size of the superlattice.[10,11] The Tamm states can dominate the optical characteristics of the superlattice[11,12] and they contribute to the in-plane conductivity.[10,13] Surface migration of dopants during the growth process was also investigated, and it reduces the electronic scattering times by about 20% and the momentum relaxation times by about 50%. Calculations are compared to experimental values measured for InP/$In_{0.53}Ga_{0.47}As$ superlattices. The theoretical values agree quite well with the experimental ones for the scattering time, whereas in respect to the momentum relaxation time theory and experiment agree only in order of magnitude. The limited success of the theory in describing the momentum relaxation time is interpreted as an indication that in modulation-doped superlattices the RPA does not provide an accurate description of the screened Coulomb potential at short distances to the ionized impurities.

II. THEORY

The RPA applied to the screened Coulomb interaction between electrons and sheets of impurities in multisubband systems is described in detail in Ref. 14. In the present work, however, the equations must be modified to take into account the difference in the values of the effective mass in the well and barrier materials. For instance, in InP/$In_{0.53}Ga_{0.47}As$ systems, the conduction band effective mass almost doubles on going from $In_{0.53}Ga_{0.47}As$ to InP. Taking account of the effective mass dependence on position on the growth axis, $m(z)$, is especially important in the case of the short-period superlattices investigated here, when the electronic wave functions penetrate the barriers. The equations will be given in effective atomic units of the bulk material comprising the quantum well layers, whereby the units of length, energy, and mass are $a_B=\epsilon\hbar^2/m^*\kappa e^2$, $\hbar^2/m^*a_B^2$, and m^*, respectively. The finite superlattice is described by subbands of energies $E(n,\boldsymbol{k}_\perp)=E_n+\frac{1}{2}k_\perp^2$; the wave functions corresponding to these energies are given by

$$\Psi_n(\boldsymbol{k}_\perp,\boldsymbol{r})=\frac{e^{i\boldsymbol{k}_\perp\cdot\boldsymbol{r}}}{\sqrt{S}}\chi_n(z),$$

where $\boldsymbol{k}_\perp$ is the in-plane wave vector and S is the area of the sample. The envelope wave functions $\chi_n(z)$ are the solutions of the Schrödinger equation

$$\left[-\frac{1}{2}\frac{d}{dz}\frac{1}{m(z)}\frac{d}{dz}+V(z)+V_H(z)+V_{XC}(z)\right]\chi_n(z) = E_n\chi_n(z),$$

where $V(z)$ is the conduction band edge energy, $V_H(z)$ is the Hartree potential, and $V_{XC}(z)$ is a local density approximation to the exchange and correlation potential.[15] The scattering rate of electrons of the Fermi energy in the ith quantum state is obtained from the Fermi golden rule

$$\frac{1}{\tau_Q^i}=\int_0^{\pi} P_i(\varphi)d\varphi,$$

where $P_i(\varphi)$ is the probability rate that an electron belonging to the ith subband, at the Fermi level, is scattered by an angle φ,

$$P_i(\varphi)=\frac{S}{\pi}\sum_{i'} m_{i'}\overline{|V_{ii'}^{\mathrm{tot}}(q_{ii'})|^2}, \tag{1}$$

$q_{ii'}$ is the scattering wave vector,

$$q_{ii'}=[k_{Fi}^2+k_{Fi'}^2-2k_{Fi}k_{Fi'}\cos\varphi]^{1/2},$$

k_{Fi} is the Fermi wave vector for the ith subband,

$$k_{Fi}^2=2m_iE_{Fi},$$

$E_{Fi}=E_F-E_i$ is the Fermi energy for the ith subband, and m_i is the effective mass for in-plane movement in the ith subband,

$$m_i^{-1}=\int\frac{\chi_i^2(z)}{m^*(z)}dz.$$

In Eq. (1), $\overline{|V_{ii'}^{\mathrm{tot}}(q)|^2}$ represents the matrix element of the screened potential that causes elastic transitions between subbands i and i', which in the RPA is given by

$$\overline{|V_{ii'}^{\mathrm{tot}}(q)|^2}=\sum_{mm'pp'}\epsilon_{ii',mm'}^{-1}(q)\epsilon_{ii',pp'}^{-1}(q)\overline{V_{mm'}^{\mathrm{ext}}(q)V_{pp'}^{\mathrm{ext}}(q)}, \tag{2}$$

where $V_{ii'}^{\mathrm{ext}}(q)$ is the two-dimensional Fourier transform of the bare scattering potential $V^{\mathrm{ext}}(q,z)$, averaged over the wave functions $\chi_i(z)$ and $\chi_{i'}(z)$, i.e.,

$$V_{ii'}^{\mathrm{ext}}(q)=\int_{-\infty}^{+\infty}\chi_i(z)\chi_{i'}(z)V^{\mathrm{ext}}(q,z)dz,$$

and the overbar denotes the statistical average over all possible uncorrelated impurity configurations. The exact result for $\overline{[V_{mm'}^{\mathrm{ext}}(q)]V_{pp'}^{\mathrm{ext}}(q)}$ depends on how the impurities are distributed along the z direction, and for a Gaussian distribution this quantity is given in Ref. 14.

In Eq. (2) $\epsilon_{ii',mm'}(q)$ is the static RPA dielectric matrix,

$$\epsilon_{ii',mm'}(q)=\delta_{im}\delta_{i'm'}+\Pi_{mm'}(q)T_{ii',mm'}(q),$$

where $\Pi_{mm'}(q)$ is the polarization matrix,

$$\Pi_{mm'}(q)=\frac{2}{S}\sum_{\boldsymbol{k}_\perp}\frac{n_{m',\boldsymbol{k}_\perp+q}-n_{m,\boldsymbol{k}_\perp}}{E_{n'}(\boldsymbol{k}_\perp+q)-E_n(\boldsymbol{k}_\perp)},$$

$n_{m,\boldsymbol{k}_\perp}$ gives the occupation probability of state $(m,\boldsymbol{k}_\perp)$, and $T_{ii',mm'}(q)$ is the Coulomb form factor,

$$T_{ii',mm'}(q)=\frac{2\pi}{q}\int_{-\infty}^{+\infty}\chi_i(z)\chi_{i'}(z)\chi_m(z')\chi_{m'}(z')\times e^{-q|z-z'|}dz\,dz'.$$

The momentum relaxation time τ_p^j associated with the jth subband was calculated by solving the following system of coupled linear equations:[16]

$$\sum_j \mathcal{K}_{ij}\tau_p^j=E_{Fi},$$

where

$$\mathcal{K}_{ij}=\delta_{ij}\sum_{j'}\mathcal{K}_{ij'}^{(1)}-\mathcal{K}_{ij}^{(2)},$$

with

$$\mathcal{K}_{ij}^{(1)}=\frac{S}{2\pi}k_{Fi}^2\int_0^{\pi}\overline{|V_{ij}^{\mathrm{tot}}(q_{ij})|^2}d\varphi$$

and

$$\mathcal{K}_{ij}^{(2)}=\frac{S}{2\pi}k_{Fi}k_{Fj}\int_0^{\pi}\overline{|V_{ij}^{\mathrm{tot}}(q_{ij})|^2}\cos\varphi\,d\varphi.$$

Using the RPA, we also calculated the scattering time due to interface roughness, substituting for $\overline{V_{mm'}^{\mathrm{ext}}(q)V_{pp'}^{\mathrm{ext}}(q)}$ in Eq. (2) the model of Prange and Nee,[17] i.e.,

$$\overline{V_{mm'}^{\mathrm{ext}}(q)V_{pp'}^{\mathrm{ext}}(q)}=\frac{\pi}{\lambda^2 S}(V_0\Delta e^{-q^2\lambda^2/4})^2\sum_{z_0}\chi_m(z_0)\chi_{m'}(z_0)\times\chi_p(z_0)\chi_{p'}(z_0),$$

where λ is the average size of the terraces, Δ is the interface roughness, V_0 is the conduction band offset at the interface, and z_0 is the position of an interface. Assuming an interface roughness of 1 monolayer,[18] and a terrace size of 65 Å for maximum interface roughness scattering,[19] the calculated scattering time is of the order of 1 ps for all states. This is about two orders of magnitude greater than the scattering time limited by Coulomb interaction, implying that scattering by interface roughness is a minor effect in our samples. Scattering by alloy disorder will also be neglected, given that the scattering time limited by alloy disorder in InP/$In_{0.53}Ga_{0.47}As$ systems is greater than ~1 ps.[20]

III. RESULTS AND DISCUSSION

A. Theoretical results

Calculations were done for InP/$In_{0.53}Ga_{0.47}As$ modulation-doped superlattices at zero temperature. The

thickness of the $In_{0.53}Ga_{0.47}As$ and InP layers was fixed at 50 Å and 40 Å, respectively. To maximize the distance between carriers and ionized donors, the donor atoms were located in the middle of the InP layers. At each doped barrier, the sheet density of donors was equal to $N_d = 3.5 \times 10^{12}$ cm^{-2}. The donor atoms were distributed along the growth axis according to a Gaussian of full width at half maximum (FWHM) 18 Å. All donors were assumed to be ionized, giving rise to an equal amount of conduction electrons, $n_S = N_d$, due to the neutrality of the structure. Figures 1(a–c) show the calculated threshold energies of the electronic subband ands the corresponding scattering times and momentum relaxation times, as a function of the number of wells N_w contained in the finite superlattice. Figure 1(a) shows that when N_w increases the energy levels generate an energy miniband of constant energy and width (~27 meV). At higher energies a two-dimensional subband is formed. The energy miniband is made up from the lowest energy $(N_w - 2)$ discrete energy subbands. The next two subbands become degenerate when N_w increases, and have their envelope wave functions completely localized in the wells at the ends of the superlattice, which characterizes them as Tamm states. The degeneracy of the Tamm states at large N_w, when the wells at the ends are isolated from each other, is a consequence of the inversion symmetry of our structure.

Figure 1(b) shows the scattering times in the individual energy levels The scattering time is shortest in the lowest energy state of the miniband, and it increases with miniband energy, because the mean electron–ionized-impurity distance increases with energy. The scattering time of the ground state and that of the state with highest energy in the miniband differ by less than 10%. The calculated average scattering time of the electronic states belonging to the miniband is 0.033 ps, whereas the Tamm states are described by a scattering time of 0.041 ps. (These scattering time values are reduced by ~10% if in all equations of Sec. II we set $m_i \equiv 1.0$. This illustrates the importance of taking into account the difference in effective mass in the well and barrier materials.)

Figure 1(c) depicts the calculated momentum relaxation times associated with the energy levels of the superlattice. Electrons belonging to the Tamm state present a shorter momentum relaxation time than electrons occupying miniband energy levels, despite the fact that the former have a longer scattering time than the latter. This is because at each collision Tamm electrons are on average deflected by a larger angle than electrons from the miniband, given that the Fermi energy for Tamm electrons is smaller than for miniband electrons [about half, as Fig. 1(a) shows]. The average scattering angle for the ith subband, $\overline{\varphi_i}$, can be calculated using $\overline{\varphi_i} = \tau_Q^i \int \varphi P_i(\varphi) d\varphi$, where $P_i(\varphi)$ is given by Eq. (1). For the structure with seven wells, the calculated value for the average scattering angle is 19° and 13° for Tamm and miniband electrons, respectively.

Since the computing time increases roughly with the fourth power of the number of subbands below the Fermi level, it is convenient to keep this number as small as possible. All calculations henceforward were done with $N_w = 7$, since at this value of N_w convergence has already been attained to a good measure, as Fig. 1 shows.

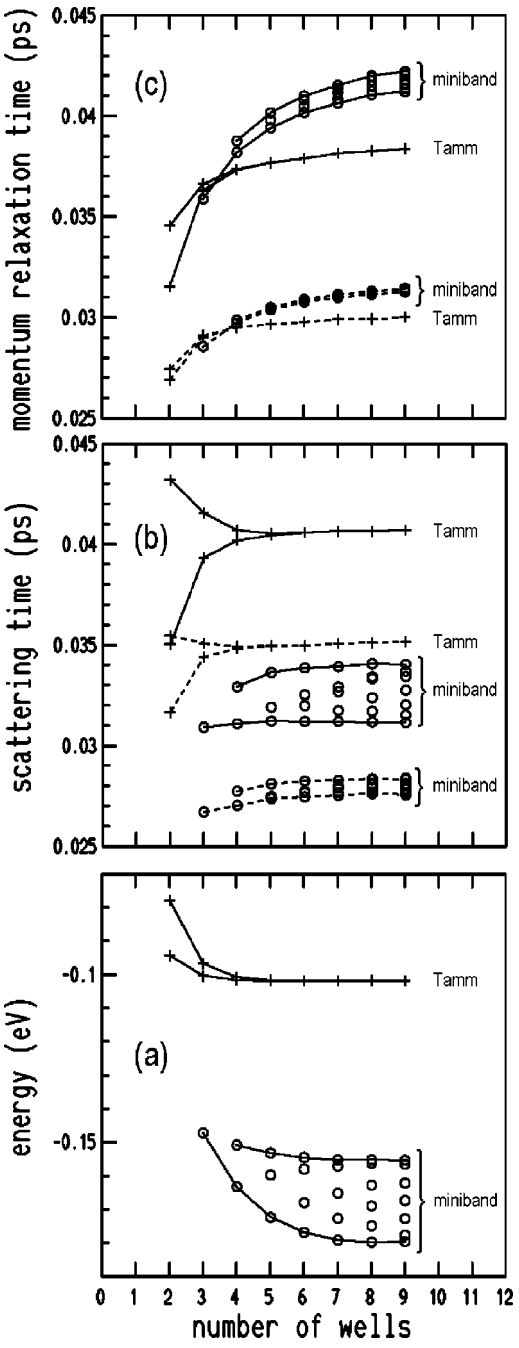

FIG. 1. Dependence on the number of wells for a 50/40 Å $In_{0.53}Ga_{0.47}As$/InP superlattice with $N_d = 3.5 \times 10^{12}$ cm^{-2}. (a) Subband energy (the origin of the energy scale was chosen at the Fermi energy); (b) single particle scattering times; (c) electronic momentum relaxation times. The miniband and Tamm states are represented by circles and crosses, respectively. The full curves represent results for the ideal structure, whereas the dashed curves are results obtained assuming an impurity segregation length of 18 Å.

Figure 2 shows the calculated threshold energies of the electronic subbands and the corresponding scattering times as a function of the sheet density of donor atoms in each InP barrier, for a structure with $N_w = 7$. Except for the doping

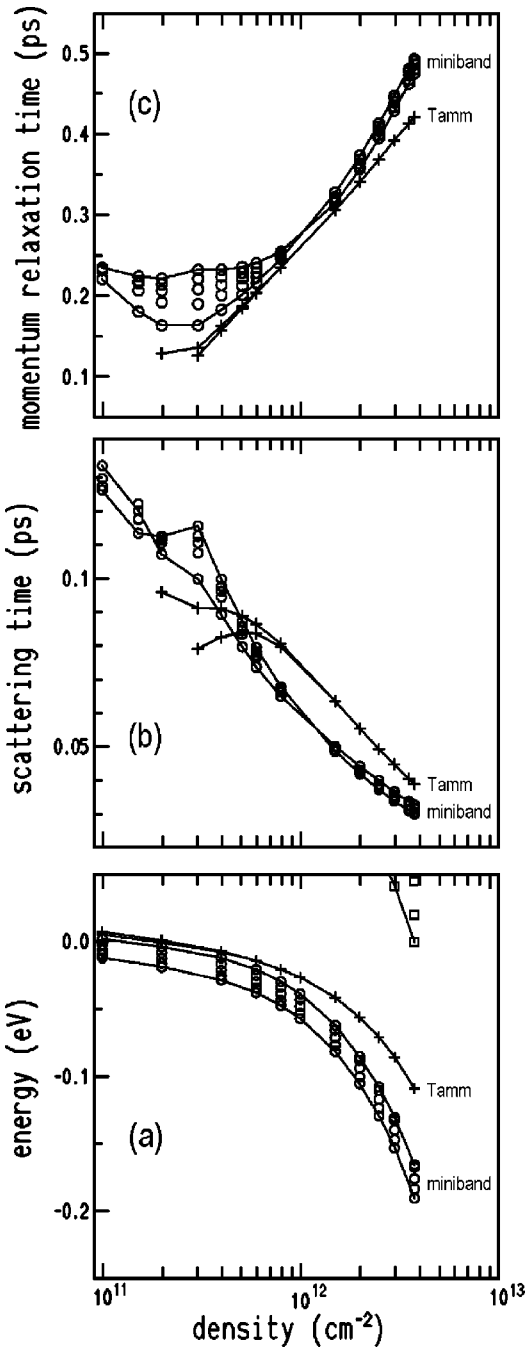

FIG. 2. Dependence on density of carriers for a 50/40 Å $In_{0.53}Ga_{0.47}As/InP$ superlattice. (a) Subband energy; (b) single particle scattering times; (c) electronic momentum relaxation times. The miniband and Tamm states are represented by circles and crosses, respectively.

density, all other parameters were maintained as before. At low n_S, the first miniband is composed from seven subbands, which are developed from the seven interacting quantum wells in resonance with each other. As n_S increases, the quantum wells at both ends of the superlattice are removed from resonance with the rest of the wells,[10] and their energy levels move toward the middle of the energy gap between minibands, forming a Tamm state. The energy width of the miniband is approximately 20 meV at $n_S=10^{11}$ cm^{-2}, and it increases to 28 meV at $n_S=5\times10^{12}$ cm^{-2}, due to the lowering of the effective barrier between wells when the doping level increases. For the Tamm state to be truly separated from the miniband, i.e., $(\hbar/2)(1/\tau_Q^{\mathrm{MB}}+1/\tau_Q^{\mathrm{T}})$, must be greater than the difference in energy between the two states. At $n_S=1.0\times10^{12}$ cm^{-2} the Tamm state is already separated from the miniband by more than ~15 meV, whereas the calculated added FWHM's of the Tamm and miniband states is only 10 meV, implying that for equal or greater values of n_S the Tamm state is fully developed.

Figure 2(b) shows that the scattering times decrease with increased doping level, due to the increasing number of scattering centers. Above $N_d=10^{12}$ cm^{-2}, the longest lived states are the Tamm states, and this is because their envelope wave functions are completely localized in the wells at the boundaries of the superlattice, and are more distant from the scattering centers than the extended miniband states.

Figure 2(c) shows that the calculated momentum relaxation times increase with increasing density of carriers; this is because with increasing n_S the Fermi energy increases, leading to smaller scattering angles. Although the scattering rate increases with increasing n_S, this is compensated by a decreasing scattering angle, the overall result being that the carrier mobility increases. An increasing mobility with increasing n_S has recently been observed experimentally in a lateral superlattice,[7] which could be explained by the same argument.

B. Experimental results

In order to test the theoretical results, magnetoresistance measurements were done on two samples, of composition $InP/In_{0.53}Ga_{0.47}As$. Both samples contained 16 $In_{0.53}Ga_{0.47}As$ layers, of thickness 50 Å each, separated by 15 InP barriers, δ-doped in their middle with Si. Sample 326 had InP barriers of thickness 50 Å, whereas sample 331 had barriers of thickness 40 Å. Transport measurements were done on etched Hall bars. More details on the samples and experimental techniques used are given in Ref. 10. The analysis of the Shubnikov–de Haas (SdH) data established that the density of donors was $\sim3.5\times10^{12}$ cm^{-2} in each barrier for both samples. Capacitance-voltage measurements indicated that the donor atoms are distributed in a layer whose characteristic width is equal to 18 Å.[21]

The quantum mobility μ_Q^i of carriers in each miniband and from the Tamm state were obtained from the damping of the SdH amplitudes at 4.2 K, using the procedure described in Ref. 9. The in-plane effective mass m_i for the ith electron species—miniband ($i=$MB) and Tamm ($i=T$) electrons—was determined from the temperature dependence of the SdH oscillations for a magnetic field applied perpendicular to the layers, as described in Ref. 22. The single particle scattering times were determined from $\tau_Q^i=m_i\mu_Q^i/e$. The density of carriers per unit area of the sample, n_i, and the transport drift mobility μ_i for the ith type of carrier were deduced from a two-carrier fit to the experimental curves $\rho_{xx}(B)$ and $\rho_{xy}(B)$, as described in Ref. 23. (Alternatively, the drift mobilities could be obtained as described in Ref. 24, i.e., by fixing the density of carriers in the miniband and Tamm

TABLE I. Sample parameters deduced from experiments. L_B is the width of the InP layers; the index MB (T) is associated with electrons in the miniband (Tamm) states; m, τ_Q, and τ_p are the electronic in-plane effective mass, scattering time, and momentum relaxation time, respectively.

Sample	L_B (Å)	m_{MB} (m_0)	m_{T} (m_0)	τ_Q^{MB} (ps)	τ_Q^{T} (ps)	n_{MB} (cm^{-2})	n_T (cm^{-2})	τ_p^{MB} (ps)	τ_p^{T} (ps)
326	50	0.0644	0.0565	0.027 ± 0.002	0.040 ± 0.002	$(46\pm3)\times10^{12}$	$(2.3\pm0.2)\times10^{12}$	0.22 ± 0.03	0.57 ± 0.02
331	40	0.0661	0.0566	0.025 ± 0.002	0.034 ± 0.002	$(47\pm3)\times10^{12}$	$(2.7\pm0.2)\times10^{12}$	0.19 ± 0.03	0.47 ± 0.03

subband at the values deduced from the SdH measurements, and using the Hall data. The two procedures yielded values in agreement with each other. However, the former procedure was preferred, given that the latter produced a much greater uncertainty in the drift mobility of the Tamm electrons. This shortcoming is peculiar to our structures, in which the densities of the two types of carrier differ by an order of magnitude.) From the drift mobility, the momentum relaxation time was obtained, using $\tau_p^i = m_i \mu_i / e$, and the results are given in Table I. The bounds to the experimental results were estimated by assuming a 5% uncertainty in all measured quantities.

C. Comparison of theory and experiment

For comparison with the experimental results, theoretical calculations were done on ideal structures described by the same parameters as the samples used in the experiment. Table II shows the results obtained from the theoretical calculations.

The theoretical scattering times for the ideal structure are 20–30 % larger than the experimental ones. A source of discrepancy between theory and experiment could be the well known effect of impurity migration toward the surface at the time of growth.[25] If we admit that in real samples surface migration occurs, then the donor atoms will be displaced from the middle of the InP barriers. To estimate the effect of surface migration we repeated the theoretical calculations assuming that the distribution of donors is displaced from the center of the InP layers by the FWHM of the donor distribution function, i.e., by 18 Å. The results are shown in Table II. Surface migration decreases the electronic scattering times, due to an increase in the Coulomb interaction between electrons and ionized donors when the donor atoms are placed nearer to the $In_{0.53}Ga_{0.47}As$ layers. The difference between theoretical and experimental values of the scattering times is essentially eliminated if surface migration is assumed.

While the theoretical and experimental scattering times agree with each other quite well, the theoretical and experimental momentum relaxation times agree only in order of magnitude. Experimentally it is found that the momentum relaxation time of the Tamm state, τ_p^{T}, is more than twice the value of the same quantity for miniband electrons, τ_p^{MB}, whereas theory gives almost equal values for τ_p^{T} and τ_p^{MB}. If surface migration is included in the theory, agreement between theory and experiment improves for τ_p^{MB}, but it becomes worse for τ_p^{T}. The general conclusion is that the theory works quite well to describe the quantum scattering times, but it does not provide an accurate description of the momentum relaxation times.

TABLE II. Theoretical values of the scattering and momentum relaxation times. The values given in parentheses were obtained assuming an impurity segregation length of 18 Å.

L_B (Å)	τ_Q^{MB} (ps)	τ_Q^{T} (ps)	τ_p^{MB} (ps)	τ_p^{T} (ps)
50	0.034 (0.030)	0.042 (0.037)	0.47 (0.26)	0.41 (0.25)
40	0.033 (0.028)	0.041 (0.035)	0.40 (0.27)	0.47 (0.29)

To explain this, one notes that the experimental value for τ_p is always an order of magnitude greater than for τ_Q. This indicates that the electrons are scattered by small angles more often than by large ones, given that only scattering events which lead to large scattering angles can contribute to τ_p, whereas scattering by any angle contributes to τ_Q. According to Sec. II, and taking into account that the scattering rates for intrasubband transitions are usually much larger than those for intersubband transitions,[26] scattering by large angles is associated primarily with matrix elements $\overline{|V_{ii}^{\mathrm{tot}}(q_{ii})|^2}$ for large values of q, i.e., it is associated with the high-frequency Fourier components of the scattering potential. Thus, a large τ_p/τ_Q ratio indicates that the Fourier amplitude of the scattering potential falls off rapidly with increasing q, which is characteristic of a long-range scattering potential. The poor agreement between theoretical and experimental values of τ_p suggests that the RPA describes poorly the high-frequency part of the Fourier spectrum of the electron-impurity interaction. By the same reasoning, one deduces that the RPA describes the low-frequency part, adequately given the good agreement between theory and experiment with respect to τ_Q, which for a long-range potential is determined mainly by the low-frequency part of the Fourier spectrum. Since the high frequencies are associated with the regions of space where the potential varies rapidly, it follows that the RPA does not describe the screened Coulomb potential in the immediate vicinity of the ionized impurities as well as it does at large distances from them. This deficiency of the RPA is the same as detected for isotropic systems, in which case the static dielectric function obtained in the RPA agrees with more elaborate approximations only in the long-wavelength region.[27] (The inaccuracy of the RPA in describing the screened potential at short wavelengths is because the RPA neglects the existence of an exchange and correlation hole around each electron participating in the dielectric screening. This leads to an estimate of

the ground state energy of the electron gas that is accurate only at high densities, i.e., when the kinetic energy is larger than the potential energy.[27])

The success of the RPA in describing accurately the scattering times, and its only limited success in describing the momentum relaxation times, has already been noted previously with regard to δ-doped layers.[8] In δ-doped layers, however, the ratio τ_p/τ_Q obtained experimentally is much smaller ($\tau_p/\tau_Q \sim 2$) than in the present case ($\tau_p/\tau_Q \sim 10$). This means that in δ-doped layers τ_p does not sample out the high-frequency part of the Fourier spectrum of the scattering potential as effectively as in the superlattices studied here. In that case, one would expect the discrepancy between experimental and theoretical values of τ_p in δ-doped layers to be smaller than for the superlattices studied here. Indeed, the discrepancy between theoretical and experimental values of τ_p in Ref. 8 is much less than in this work, which fits well into the hypothesis that the RPA does not describe accurately the short-range component of the Coulomb interaction in layered structures.

IV. CONCLUSION

The electronic scattering times and the momentum relaxation times in modulation-doped superlattices were calculated, using the RPA to describe the screening of the scattering potential. The scattering and momentum relaxation times were measured for InP/$In_{0.53}Ga_{0.47}As$ superlattices. Theoretical calculations done on structures with the same parameters as used in the experiments reproduce the experimental scattering times quite well; however, the theoretical and experimental values of the momentum relaxation times agree only in order of magnitude. It is suggested that the source of the discrepancy between theory and experiment is the inaccuracy of the screened potential in the RPA at short distances from the ionized impurities.

ACKNOWLEDGMENTS

This work was supported by FAPESP, under Contract Nos. 99/10359-7 and 99/12694-8, and CNPq, under Contract No. 306335/88.

[1] L. Esaki and R. Tsu, IBM J. Res. Dev. **14**, 61 (1970).
[2] C. Waschke, H. G. Roskos, R. Schwedler, K. Leo, H. Kurz, and K. Köhler, Phys. Rev. Lett. **70**, 3319 (1993).
[3] A. Sibille, J. F. Palmier, H. Wang, and F. Mollot, Phys. Rev. Lett. **64**, 52 (1990).
[4] C. Rauch, G. Strasser, K. Unterrainer, W. Boxleitner, E. Gornick, and A. Wacker, Phys. Rev. Lett. **81**, 3495 (1998).
[5] K. J. Luo, H. T. Grahn, K. H. Ploog, and L. L. Bonilla, Phys. Rev. Lett. **81**, 1290 (1998).
[6] Luis Brey, Phys. Rev. Lett. **81**, 4692 (1998).
[7] A. Majumdar, L. P. Rokhinson, D. C. Tsui, L. N. Pfeiffer, and K. W. West, Appl. Phys. Lett. **76**, 3600 (2000).
[8] Guo-Qiang Hai, N. Studart, and F. M. Peeters, Phys. Rev. B **52**, 8363 (1995).
[9] A. B. Henriques, L. C. D. Gonçalves, N. F. Oliveira, Jr., P. L. Souza, and B. Yavich, Phys. Rev. B **55**, 13 072 (1997).
[10] A. B. Henriques, L. K. Hanamoto, P. L. Souza, and B. Yavich, Phys. Rev. B **61**, 13 369 (2000).
[11] A. B. Henriques, Appl. Phys. Lett. **78**, 691 (2001).
[12] A. B. Henriques, R. F. Oliveira, P. L. Souza, and B. Yavich, Physica B **298**, 320 (2001).
[13] A. B. Henriques (unpublished).
[14] A. B. Henriques, Phys. Rev. B **53**, 16 365 (1996).
[15] L. Hedin and B. Lundqvist, J. Phys. C **4**, 2064 (1971).
[16] E. D. Siggia and P. C. Kwok, Phys. Rev. B **2**, 1024 (1970).
[17] R. E. Prange and Tsu-Wei Nee, Phys. Rev. **168**, 779 (1968).
[18] A. P. Roth, P. Levesque, R. W. G. Syme, D. J. Lockwood, G. C. Aers, T. S. Rao, and C. Lacelle, J. Appl. Phys. **80**, 4033 (1996).
[19] P. Roblin, R. C. Potter, and A. Fathimulla, J. Appl. Phys. **79**, 2502 (1996).
[20] G. Bastard, J. A. Brum, and R. Ferreira, Solid State Phys. **44**, 229 (1991).
[21] L. K. Hanamoto, A. B. Henriques, C. Tribuzy, P. L. Souza, and B. Yavich (unpublished).
[22] A. B. Henriques, P. L. Souza, and B. Yavich, Semicond. Sci. Technol. **16**, 1 (2001).
[23] J. S. Kim, D. G. Seiler, and J. R. Ehrstein, J. Appl. Phys. **80**, 4425 (1996).
[24] E. Skuras, A. R. Long, B. Vögele, M. C. Holland, C. R. Stanley, E. A. Johnson, M. van der Burgt, H. Yaguchi, and J. Singleton, Phys. Rev. B **59**, 10 712 (1999).
[25] E. F. Schubert, *Doping in III-V Semiconductors* (Cambridge University Press, Cambridge, 1993), p. 243.
[26] S.-C. Lee and I. Galbraith, Phys. Rev. B **59**, 15 796 (1999).
[27] D. Pines and P. Nozières, *The Theory of Quantum Liquids*, Vol. 1 (Addison-Wesley, New York, 1989), Chap. 5.